Structure development of low-density polyethylenes during film blowing : a real-time wide-angle X-ray diffraction study

Structure Development of Low-Density Polyethylenes During Film Blowing: A Real-Time Wide-Angle X-ray Diffraction Study

Martin van Drongelen, Dario Cavallo, Luigi Balzano, Giuseppe Portale, Iakovos Vittorias, Wim Bras, Giovanni C. Alfonso, Gerrit W. M. Peters*

We studied experimentally the structure development during film blowing for three different low-density polyethylenes at four different processing conditions. For this, we combined blown film extrusion with in situ X-ray diffraction at a synchrotron radiation beam line. The measurements were performed at rheological similar conditions at the die exit, with each grade possessing different molecular properties in terms of molecular weight distribution and branching content. The development of crystallinity and molecular orientation was determined as function of the distance from the die. It is shown that this approach provides a valuable method to study structure evolution during film blowing and can be used to validate results from numerical models and help to improve and/or extend these models.

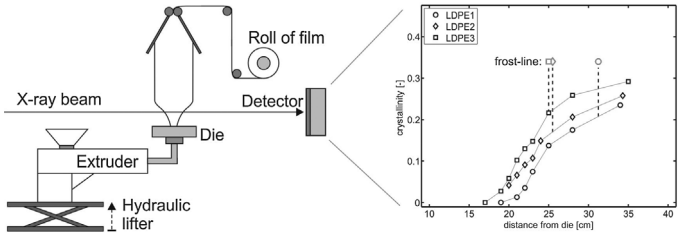

Prof. G. W. M. Peters, M. van Drongelen
Department of Mechanical Engineering, Materials Technology Institute, Eindhoven University of Technology, P.O.Box 513, 5600 MB, Eindhoven, the Netherlands
E-mail: g.w.m.peters@tue.nl
Dr. D. Cavallo, Prof. G. C. Alfonso
Department of Chemistry and Industrial Chemistry, University of Genova, via Dodecaneso 31, 16146 Genova, Italy
Dr. L. Balzano
DSM Material Science Center, Urmonderbaan 22, Geleen 6167 RD, The Netherlands
Prof. G. W. M. Peters, Dr. L. Balzano
Dutch Polymer Institute (DPI), P.O. Box 902, 5600 AX Eindhoven, the Netherlands
Dr. G. Portale, Dr. W. Bras
DUBBLE CRG BM26@ESRF, Netherlands Organization for Scientific, Research (NWO), European Synchrotron Radiation Facility, BP 220, F-38043 Grenoble Cedex, France
Dr. I. Vittorias
Basell Polyolefine GmbH, a LyondellBasell company, R&D, Polymer Physics & Characterization, Industriepark Hoechst, C657, 65926 Frankfurt a. M., Germany

1. Introduction

The blown film extrusion process is extensively used in the packaging industry to make large volumes of polymer films. Because of the large, worldwide demand for these kinds of products, the manufacturing speed is high and, consequently, shaping the product involves high deformation rates and steep thermal gradients. Due to the considerable amount of research dedicated to polymer processing in the last few decades, it has become well known that the conditions applied during the production process, together with the molecular features of the polymer resin, determine the final microstructure, i.e., the crystalline and amorphous morphology and orientation thereof[1–6] and, thus, the final mechanical, optical and barrier properties.[7–9] However, the coupled relations between these quantities are often complex and rather difficult to seperate.

Some of the most common materials used in film blowing are high- and low-density polyethylenes, HDPE and LDPE, respectively. For these ethylene-based polymers,

DOI: 10.1002/mame.201400161

depending on the material and the processing conditions, different structures of organized lamellae are formed during crystallization.[10–12] In the absence of flow, spherulitic structures are formed by lamellae that grow in radial direction, with the growth rate being a function of temperature and pressure. As a result of stretching of the melt, row nucleated or fibrillar (shish-kebab) structures may develop. The radial growing lamellae are either twisted at low stress levels or straight at higher stress levels.[13] During film blowing, the conformation of the molecules is strongly affected by biaxial stretching. Typically, the final film consists of a mixture of the lamellar structures mentioned.[11,14] In the machine direction, defined as the production direction, e.g., from the die toward the niprolls, the stretch is defined by the ratio between the pick-up speed of the niprolls and the average feeding speed at the die (defining the take-up ratio, the TUR), in the cross-machine direction the stretch is defined by the bubble inflation, i.e., the ratio between the final bubble diameter and the die diameter (defining the blow-up ratio, the BUR).

The morphology of the blown film has been extensively studied by means of different experimental methods, such as for instance differential scanning calorimetry (DSC),[7] scanning/transmission electronic microscopy (SEM/TEM),[15] birefringence[16] or X-ray scattering techniques.[7,17] However, these measurements were carried out post mortem. They can be used to modify the process by trial and error, which can be expensive and time consuming since experiments need to be repeated several times before optimal processing conditions are found. Therefore, a systematic study of the morphology development, i.e., the crystallization kinetics along the film line, which can be achieved by using accurate on-line methods, is considered to be of great importance for a better understanding of the production processes and will ultimately lead to improving and fine-tuning of the film properties. There are a number of models that describe the film blowing process,[18–23] of which the most detailed ones are published recently. The experimental results we obtained can be used to validate or improve/extend such models.

In film blowing lines in industry, online measurements of the film quality are established by means of optical quality check in order to locate surface defects such as shark-skin or to detect the occurrence of melt fracture. On a smaller scale, several researchers report on real-time measurements combined with different methods such as SALS,[24] Raman spectroscopy[25] or birefringence.[15,26] Among various characterization methods, X-ray diffraction techniques such as Small Angle X-ray Scattering (SAXS) or Wide Angle X-ray Diffraction (WAXD), provides for a direct measurement technique to obtain the crystallinity and molecular orientation within a sample. For practical reasons, on-line structure analysis using X-ray based methods, was still reserved for lab-scale environments.[27,28] Combining a pilot-plant film blowing setup with X-ray leads to many impracticalities and limits the accessibility of the blown film line because of the presence of radiation sources. The experiments reported in this work were made possible by combining a medium scale film blowing setup with a synchrotron radiation beam line.

Due to the combination of a high X-ray flux and a high degree of collimation of the X-ray beam and an advanced detector, structure formation could be examined in situ. In this way, a combination of different machine settings, relevant for processing conditions, could be explored within a short amount of time and with an accuracy beyond the capacity of laboratory sources.[29] The goal of the present study is to investigate the crystallinity and molecular orientation along the film line for different processing conditions and materials. Three different grades of LDPE are investigated for different blow-up ratios and take-up levels. For a better understanding of the structure evolution during processing in terms of the molecular properties, an extensive material characterization is provided by using oscillatory rheology and gel-permeation chromatography (GPC).

2. Materials and Methods

2.1. Materials

All tested samples are commercial low-density polyethylene (LDPE) grades from the Lupolen product family of LyondellBasell. These samples were selected because they allow for the investigation of the role of molecular features in the crystallization behavior under complex conditions. The LDPEs vary in molecular weight distribution (MWD), long-chain branching (LCB), thermal and rheological properties.

2.2. Molecular Characterization

The molecular weight distribution of the studied polymers was determined by gel-permeation chromatography, GPC, using a Polymer Laboratory PL 210, at 140 °C. A Wyatt DAWN EOS was used as detector to perform Multi-angle-laser-light scattering (MALLS) measurements in order to determine the long-chain branching. Samples were dissolved in trichlorobenzene, TCB, (0.04 wt.-%) and eluted at 0.6 ml $\cdot \min^{-1}$. For MALLS calibration, linear PS and PE standards were used.

2.3. Thermal Characterization

Differential scanning calorimetry was used to quantify the melting and quiescent crystallization behavior, using a DSC Q2000 apparatus (TA Instruments). The sample was heated with 20 °C $\cdot \min^{-1}$ from −10 to 200 °C and subsequently

cooled with the same rate to −10 °C and again heated to 200 °C. The melting peak (of the 2nd heating run), T_m, the crystallization peak, T_c, and the onset of crystallization (temperature where heat-flow decreases below the baseline), $T_{c,onset}$, are determined using the TA Universal Analysis 2000 software.

2.4. Rheological Characterization

The granulate samples were compression-molded at 200 °C and at 200 bar for 4 min to approximately 1 mm thick plates, from which the samples were cut out. The rheological characterization was performed in an Anton-Paar MCR301 rheometer. Dynamic oscillatory shear measurements were performed at three temperatures, 150, 190, and 210 °C. Curves were shifted to a mastercurve at $T = 190$ °C and the activation energy, E_a, was calculated. Elongational viscosity measurements were done at 150 °C using a mounted SER fixture[30] with strain rates 0.05, 0.1, 0.5, 1, 5, and 10 s^{-1}.

2.5. Film Blowing Setup

A Collin Blown Film Unit type 180–400 and extruder were mounted on the X-ray beamline. A picture of the experimental hutch with the setup placed in position is shown in Figure 1. The used die diameter and die gap were 50 and 0.8 mm, respectively. The processing conditions used are given in Table 2. Since film blowing is a complex problem and we wanted to make the experiments as much as possible "comparable" we tried to keep the most important conditions the same. This includes the throughput, the BUR and TUR values (i.e., the biaxial stationary stretched state) and, finally, the shear history of the materials before it leaves the die. For the latter we choose the Weissenberg number (the product of relaxation time and shear rate) to be similar for the different grades. Therefore, the extrusion temperature was set to 200 °C for all zones for the grade(s) with the high viscosity (grade 1 and 2) and to 180 °C for the low viscosity grade (grade 3), respectively. In this way, the viscoelastic behavior at the exit of the die is similar for the three grades for similar other processing conditions. Die exit velocity has been calculated considering a melt density of 0.768 for grade 3 and 0.757 g $\cdot$ cm^{-3} for grade 1 and 2, respectively.[31]

The processing conditions were tuned in order to approximate a similar set of blow-up ratios (BUR) and take-up ratios (TUR) for all grades. Take-up ratio is defined as the ratio of the take-up velocity (at the niprolls) with respect to the average speed at the die, while blow-up ratio is defined by the ratio of the final bubble diameter with respect to the diameter of the die.

Each material was blown in four different conditions following a combinatorial approach, i.e., for each of the two BUR values two TUR levels were employed.

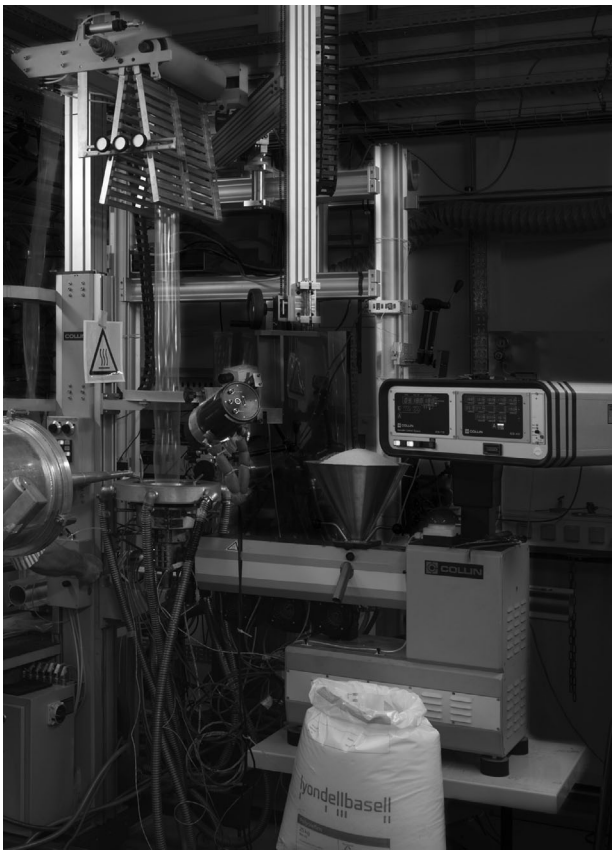

Figure 1. Blown film unit (left) and extruder (right) mounted at BM26B, DUBBLE@ESRF. (X-ray detector not yet into position).

2.6. Particle Tracing

To identify the velocity of the film at a certain distance from the die, and the time to reach that position, movies of the bubble were collected for each processing condition by means of a CCD camera and analyzed using the Kinovea software package. For that purpose, pieces of black tape were placed on the film surface as a marker and tracked as a function of time. As an example, some movie frames are shown in Figure 2. Due to a slight misalignment of the die, a asymmetry is observed in the bubble shape.

The position of the tracker given by the software, i.e., pixel versus time, was first converted into distance from the die as a function of time by means of a calibration image, and then smoothed. The axial velocity profile, v_z, as function of distance from the die, z, was obtained by calculating the time derivative of the data. For each experimental condition, data from three different movies was averaged and fitted with the following expression:

$$v_z(z) = a + \frac{b}{1 + \exp\left(-\frac{z-c}{d}\right)}, \quad (1)$$

Table 1. Processing conditions. Data in column marked by (*) is given only when available.

Experiment	Bubble diam. [mm]	Throughput [g × min^{-1}]	Take-up vel. [m × min^{-1}]	TUR [–]	BUR [–]	Frost-line height* [cm]	Film thickness [μm]
1-BURL-TURL	95	14.4	1.30	8.2	1.9	31.25	41
1-BURL-TURH	95	14.4	2.66	16.8	1.9		41
1-BURH-TURL	124	14.2	1.31	8.4	2.5	23.75	54
1-BURH-TURH	121	14.4	2.66	16.8	2.4		53
2-BURL-TURL	95	14.6	1.36	8.5	1.9	25.50	41
2-BURL-TURH	95	14.0	2.76	17.9	1.9		41
2-BURH-TURL	127	14.6	1.34	8.3	2.5	20.00	56
2-BURH-TURH	118	14.2	2.76	17.7	2.4		51
3-BURL-TURL	95	13.8	1.32	8.8	1.9	25.00	41
3-BURL-TURH	95	14.4	2.78	17.8	1.9		41
3-BURH-TURL	131	13.8	1.32	8.8	2.6	17.00	57
3-BURH-TURH	131	14.2	2.76	18.0	2.6		57

where a, b, c, and d are all fitting parameters. An example of the measured and fitted velocity profile is plotted in Figure 3.

The particle tracing method was mainly used to acquire the axial position of the frost-line. This is the distance from the die where a constant axial velocity of the fitted profile is achieved, i.e., the melt has changed into a solid. This transition is mainly determined by external cooling of the extruded melt. In practice, a cooling ring is mounted on top of the die with the dual function to increase the cooling rate and stabilize the blown film. For the film blowing setup used, the air flux control was limited, leading to either a frost-line located very close to the die (at high air flux), or, in the absence of air flux, at a large distance from the die. Since the scope of this work was to measure the structure evolution along the machine direction, MD, at multiple distance levels from the die and below the frost-line, no additional air cooling was used. Since the vertical displacement of the extruder was limited, a maximum travel range of ≈25 cm, the X-ray beam could not be directed close to the frost-line height for high TUR conditions (see next section for more details about the setup). Additionally, the camera could not capture a sufficient amount of bubble surface to determine the frost-line height. As a result, the frost-line height could only be analytically determined for the conditions with low take-up ratio, i.e., low film speed, where solidification still took place at relatively close distance from the die. Even so, the results of the experiments at lower TUR still provide valuable information to discuss structure evolution with respect to the frost-line level.

2.7. X-Ray Experiments and Framework for Data Analyses

The film blowing experiments were combined with 2D wide-angle X-ray diffraction (WAXD) measurements at the Dutch-Belgian (DUBBLE) beamline BM26 of the European Synchrotron Radiation Facility in Grenoble, France.[32,33] The vertical position of the extruder with respect to the X-ray beam could be adjusted by raising the die and extruder step-by-step through a manually operated hydraulic lift table. The adopted setup is shown schematically in Figure 4. The source-ray photon wavelength was set to 1.033 Å, the X-ray beam was 300 μm in diameter.

Measurements were done at ten die-beam distances between 15 and 40 cm. In each position, 10 WAXD patterns

Table 2. Materials studied. Density, weight-averaged molecular weight, $\overline{M}_w$, and polydispersity, $\overline{M}_w/\overline{M}_n$ with $\overline{M}_n$ the number averaged molecular weight and average long-chain branching, LCB/1000 CH_2, from GPC-MALLS as calculated by the Zimm-Stockmayer model for trifunctional branches. Melting temperature, T_m, and crystallization temperature, T_c, are determined by DSC at a cooling rate 20 °C · min^{-1}.

Material	Density [g × cm^{-13}]	$\overline{M}_w$ [kg × mol^{-1}]	$\overline{M}_w/\overline{M}_n$ [–]	LCB/1000 CH_2	T_m [°C]	T_c [°C]	$T_{c,onset}$ [°C]
LDPE1	0.923	390	8	0.35	109	97	101
LDPE2	0.927	200	7	0.24	113	100	103
LDPE3	0.923	200	5	0.29	112	96	100

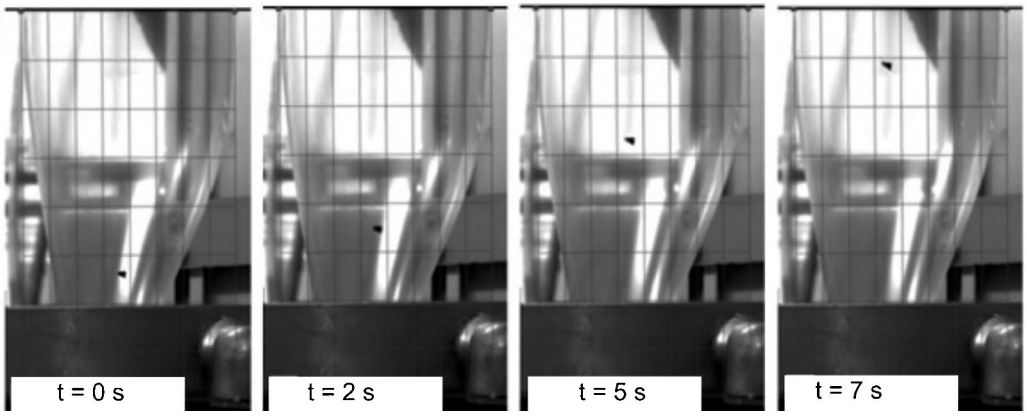

Figure 2. Example of marker position in time, machine direction is vertical.

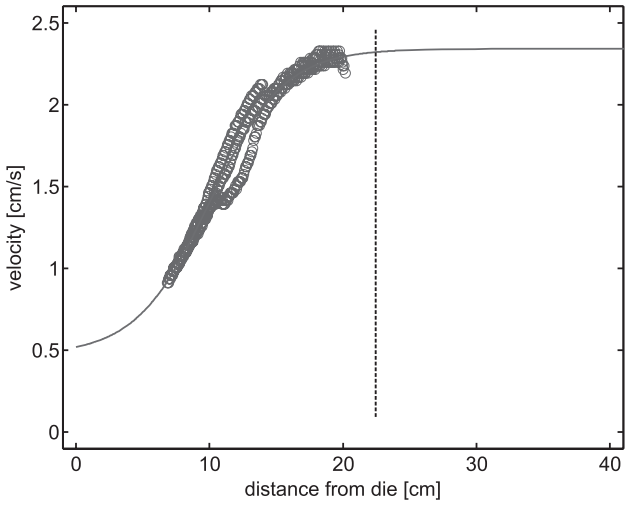

Figure 3. Measurements for two markers (symbols) and fitted average velocity profile (solid line) as function of distance from the die. The dashed vertical line indicates the frost-line position.

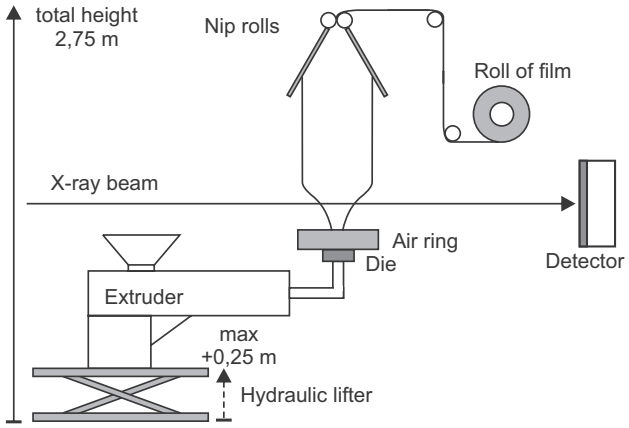

Figure 4. Schematic setup of the film blowing device, X-ray beam and detector position.

were acquired with an exposure time of 10 s, which resulted in a time average of about 2 min. For each height step in a given experiment, crystallinity and molecular orientation was evaluated as the average of at least three patterns. With an average of about 50 m, the exposure time used provided a clear diffraction pattern. All patterns were collected by means of a CCD detector (Photonic Science, UK) with 1024×1024 pixels of 97.65×97.65 μm placed at approximately 170 mm from the bubble surface. All WAXD data were background subtracted and integrated using the software package FIT2D (ESRF, France). The X-ray crosses the bubble twice and, depending on the bubble diameter, the diffracted patterns of the front and back face of the bubble can be either conjoined or separated. In our experiments, we have taken care that the WAXD patterns are sufficiently separated. From the blown bubble, only the diffraction from the second wall was used throughout the whole of the analysis. The crystallinity level was determined by comparing the area underneath the radially integrated diffraction peaks of the orthorhombic unit cell of polyethylene ($d = 4.17$ and 3.70 Å), to the total area underneath the diffracted pattern. The amorphous halo, required to evaluate the crystalline contribution, was obtained from a pattern of the molten polymer acquired at a short distance from the die. For the crystallinity a standard deviation of 1.5% was obtained, a typical value for this type of calculation.

Crystal orientation along MD has been estimated from the reflections of the (110) and (200) Bragg peaks, after removal of the scattering from amorphous material, by two different methods: the relatively simple method, based on the full-width-at-half-maximum (FWHM) of the (110) reflection and the more detailed Hermans' orientation factor. The use of both methods allows us to monitor both the overall orientation evolution and, in more detail, the orientation of the a-, b-, and c- crystalline axes of the orthorhombic unit cell of polyethylene. For both cases, the

machine direction is considered as 0° and the transverse direction as 90°. In the following, both methods are briefly discussed.

2.8. Method I: Full Width at half Maximum

The intensity distribution of the (110) reflection is used to quantify the overall orientation level by fitting two Lorentzian functions to the azimuthal intensity profiles. The full-width-at-half-maximum (FWHM) of the curve is a measure for the degree of orientation, where a lower value, i.e., a smaller radial extent, indicates a higher level of orientation. In the case of a twisted lamellar structure, or Type I morphology, a summation of two coupled functions is required; the a- and c-crystallographic axis continuously twist around the b-axis, resulting in a (≈50°-spaced) double peak profile,[13] such as displayed in Figure 5.

The expression for each fitted Lorentzian function is given by:

$$I_L(\beta) = A + \frac{B\gamma}{(\beta - \beta_0)^2 + \gamma^2}, \quad (2)$$

where A and B are scaling parameters, β_0 the center of a peak and γ is a parameter specifying the width. Now, for the FWHM it simply follows that:

$$\text{FWHM} = 2\gamma \quad (3)$$

For reasons of data interpretation, the obtained FWHM is converted in radians and plotted as 1/FWHM, where a higher value represents a higher level of orientation. We found a standard deviation of 4% on the average value of the FWHM.

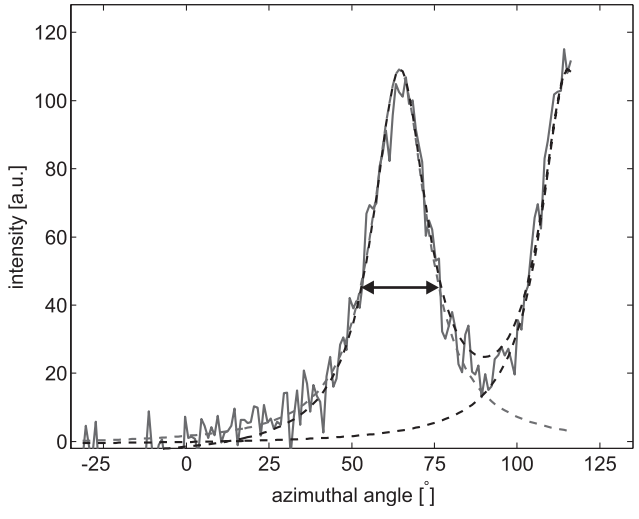

Figure 5. Example of fitting the Lorentzian curves (dashed lines) to the azimuthal scattering profile (thick line) to determine the FWHM for a Type I oriented structure.

2.9. Method II: Hermans' Orientation Factor

A second approach to determine the orientation is formalized by using the Hermans' orientation factor.[34,35] An important constraint of this method for 2D WAXD patterns is the validity of the assumption that rotational symmetry is found in the machine direction, e.g., such as present in fiber production. In the ideal case, pole figures are measured to acquire a unique solution for the distribution of each crystallographic axis.[36] There is no need to argue that this is impossible for the current type of experiment. In this work, we deal with bi-axially stretched films and, at first sight, Hermans' orientation factor does not qualify for determination of the molecular orientation. Nevertheless, since the stretch in the machine direction exceeds the level of stretch in the lateral direction by at least one order of magnitude, it is assumed valid to use this approach without significant miscalculations. Application of Hermans' orientation factor is further supported by investigating the crystal plane orientation (CPO) parameter, which is defined as the ratio between the peaks of the (200) and (110) reflection.[37] In the case of strongly decreasing CPO values, the occurrence of uniplanar orientation of the (200) plane in the direction perpendicular to the film surface would prevent scattering of this plane due to non-Bragg conditions.

The orientation factor is denoted by f_H, which is defined as

$$f_H = \frac{3\langle\cos^2\phi\rangle - 1}{2}, \quad (4)$$

where ϕ is the angle between the crystallographic axis and a reference axis, e.g., the machine direction, and $\langle\cos^2\phi\rangle$ is the average value of the cosine squared of this angle. The orientation factor f_H is zero for a fully random orientation, and 1.0 or −0.5 for a sample fully oriented parallel and perpendicular to the machine direction, respectively.

For the orthorhombic symmetry found in the unit cell of polyethylene, the orientation factors can be calculated from the ratio of the measured reflection of the (110) and (200) planes. The reflection of the (020) plane is calculated based on the relations demonstrated by Wilchinsky.[38] The a- and b-axis orientation (f_a, f_b) can now be obtained by substituting $\langle\cos^2\phi_{200}\rangle$ or $\langle\cos^2\phi_{020}\rangle$ in the expression for f_H, (Equation 4), respectively. Since orthogonal symmetry applies, the total of all orientation factors adds up to 1 and the value for f_c follows automatically. Typically, we found a standard deviation of 0.04 on the average value of the orientation factor, f_H.

3. Results and Discussion

The evolution of the microstructure within the blown film is investigated along the machine direction for multiple

processing conditions and materials. Different structures of organized lamellae may form during crystallization.[10,11,12] Hence, two scenarios for flow-induced structure formation are briefly discussed, followed by the results of several characterization techniques which were used to acquire, in detail, the structural features. For clarity we present a stepwise analysis of the data. The effect of different processing conditions on the evolution of crystallinity is evaluated first, followed by the level of orientation, which is quantified by both, the FWHM approach and the Hermans' orientation factor. The FWHM method will provide a measure for the molecular orientation on the arbitrary unit scale, in addition, use of the Hermans' orientation factor allows us to study the evolution of orientation in a more detailed level. Since the results of different processing conditions on the orientation are very similar for the three grades, the latter is only discussed for LDPE1. Finally, the effect of different molecular architectures is discussed by comparing the structure evolution, i.e., the development of crystallinity and orientation, for the different polymers under similar processing conditions.

3.1. Background

During the film blowing process and for a given flow condition at sufficiently high temperature, the molecules of the high-end tail of the molecular weight distribution, possessing long relaxation times, are able to orient into fibrous crystals in the direction of flow. Subsequently, lamellae grow laterally outward from these nucleation sites, resulting in the well known shish-kebab structure. The most commonly accepted physical picture of oriented structure formation in polyethylene films is given by the row-nucleated model,[10] which is also used for the interpretation of the data presented in this work. To a large extend, the magnitude of stress imposed on the polymer melt, which is equivalent to the molecular stretch,[39] controls the crystallization behavior.[40] At low stresses, the lamellae, growing perpendicular to the shish, form twisted ribbons with a preferential orientation of the crystalline *a*-axis toward the machine direction, which is also known as the (Keller-Machin) Type I structure, displayed in Figure 6a. At high stresses, the growing lamellae form regularly folded chains, with the c-axis (or chain direction) parallel to MD; a structure which is also known as Type II, schematically represented in Figure 6b. For both cases, a schematic 2D WAXD pattern is included. Considering the level of processing conditions close to resembling industrial values, Type II structures have only been observed in HDPE blown film.[41] For different grades of LDPE and LLDPE, combinations of spherulitic and oriented Type I morphologies can be expected depending on the deformation induced stress level, a function of the molecular architecture.[11,12]

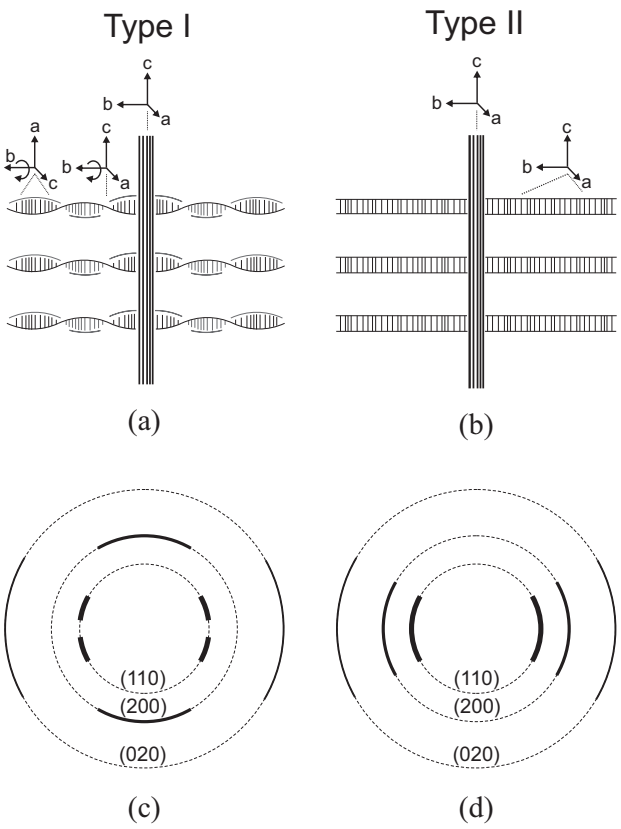

Figure 6. Schematic picture and typical WAXD pattern of oriented polyethylene of twisted (a,c) and untwisted/regular lamellae (b,d), machine direction is vertical.

The influence of branching content on (flow-induced) crystallization is less well documented, especially in the case of film blowing applications. In short, branching content in polyethylenes can be composed of long-chain branched (LCB) and short-chain branched (SCB) chains. An increase of SCB will reduce density and maximum crystallinity since less perfect crystalline lamellae can be formed.[42] LCB increases shear thinning and orientability of the materials, the level of LCB can therefore have a large impact on the final morphology of the film. The focus of this research is more on the role of LCB on structure evolution during film blowing. The effect of SCB is only slightly touched on since, based on the density differences, we expect LDPE2 to have a lower content of SCB. Multiple characterization techniques were selected to identify the molecular details and processing related properties for each of the selected materials, i.e., the molecular weight distribution (MWD), the long chain branching content (LCB), the viscosity, and elongational properties. Sufficient knowledge on the molecular architecture is of importance in order to anticipate on the differences in structure evolution during the actual film blowing process. Moreover, a much larger set of materials would be required for a

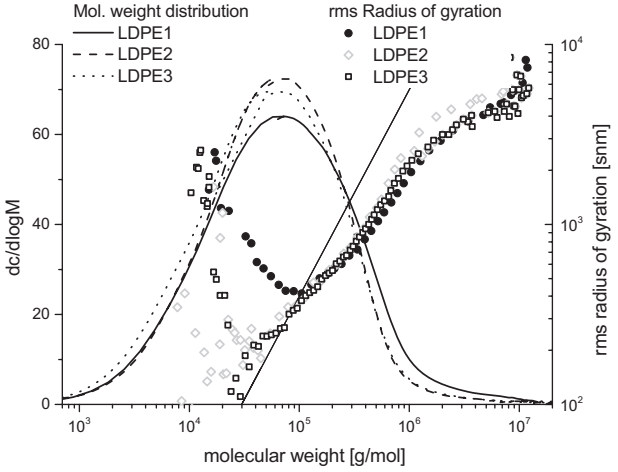

Figure 7. Molecular weight distribution and root mean square (rms) radius of gyration, R_g, measured as determined by GPC-MALLS. The solid line represents the reference rms R_g as a function of molecular weight for a linear polymer. The higher the deviation between measured and reference, the higher the LCB degree.

comprehensive, systematic study on the combined effect of LCB and SCB and much more experiments need to be done (future work).

3.2. Material Characterization

3.2.1. Molecular Characterization and Thermal Properties

The most important properties of these materials, determined with DSC and GPC-MALLS, are given in Table 2.

From the GPC-MALLS results, depicted in Figure 7, it can be concluded that LDPE1 has a significantly broader MWD, a larger fraction of high molecular weight and higher LCB degree. LDPE2 and LDPE3 exhibit similar MWD with LDPE3 having slightly more low molecular weight chains. With regard to LCB, quantified by the deviation of measured radius of gyration, R_g, with respect to the linear reference, the LDPE2 has the lowest branching degree of all three samples, even though LDPE2 shows a significant increase in LCB concentration at ultra-high molecular (UHM) weights ($10^6 < M < 10^7$). Since a high UHM weight fraction is needed for the formation of flow-induced structures, it is expected for LDPE1 to show a relatively high amount of orientation compared to the other LDPE grades.

3.2.2. Rheological Characterization

The storage and loss moduli of the three grades are given in Figure 8, the phase angle versus complex modulus (van Gurp-Palmen plot) and the dynamic viscosity are shown in Figure 9. From these data the corresponding Maxwell spectra were determined, see Figure 10a. LDPE1 has, in agreement with the measured MWD, a broader rheological spectrum and the highest viscosity of all three grades. LDPE2 and LDPE3 have, mainly due to the narrower MWD, a narrower spectrum. The difference in flowability between the latter two is due to the higher LCB degree of LDPE3 and is mainly observed for the lower dynamic viscosity. The difference in LCB is not manifested in the van Gurp-Palmen plot (phase lag vs. complex modulus); LDPE2 and LDPE3 show almost the same behavior, see Figure 9a, while GPC-MALLS reveals significantly higher LCB degree for LDPE3. This is, however, typical for LDPE's; due to the complex branched structure, linear rheology is not sensitive enough to elucidate structural differences. The high branching degree is the main relevant parameter during the extensional flow, since it is believed that this dominates the material behavior during film blowing. Elongation viscosity curves measured at $T_{ref} = 150\,^{\circ}C$ are given in Figure 11a. Only a small difference is found in the linear regime. For all materials a clear viscosity upturn is observed

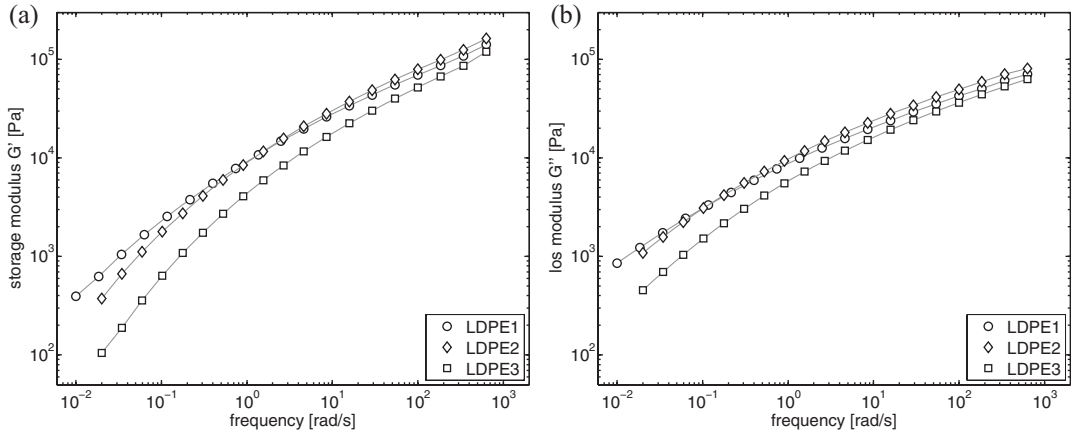

Figure 8. Storage (a) and loss modulus (b) for all LDPE's, $T_{ref} = 190\,^{\circ}C$.

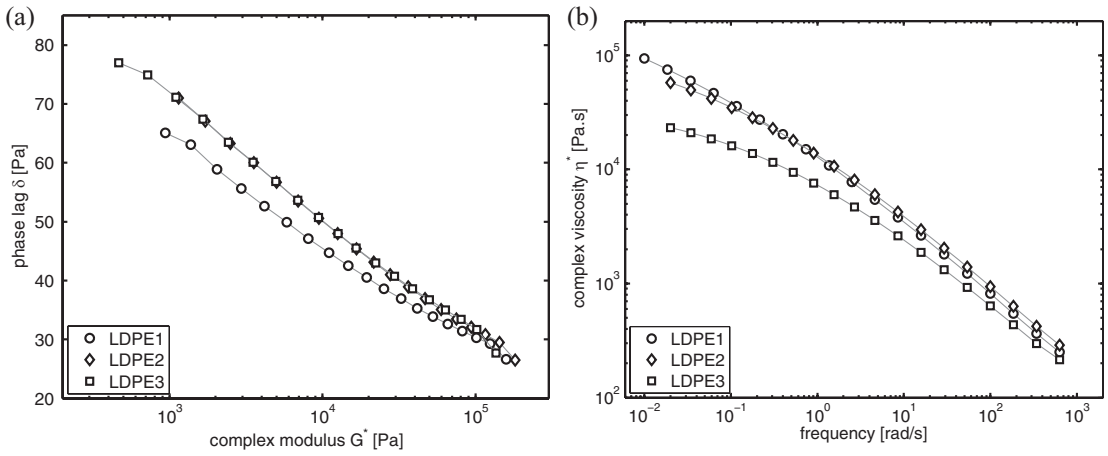

Figure 9. Phase angle versus complex modulus (a) and complex viscosity for all LDPE's, $T_{ref} = 190\ ^{\circ}C$.

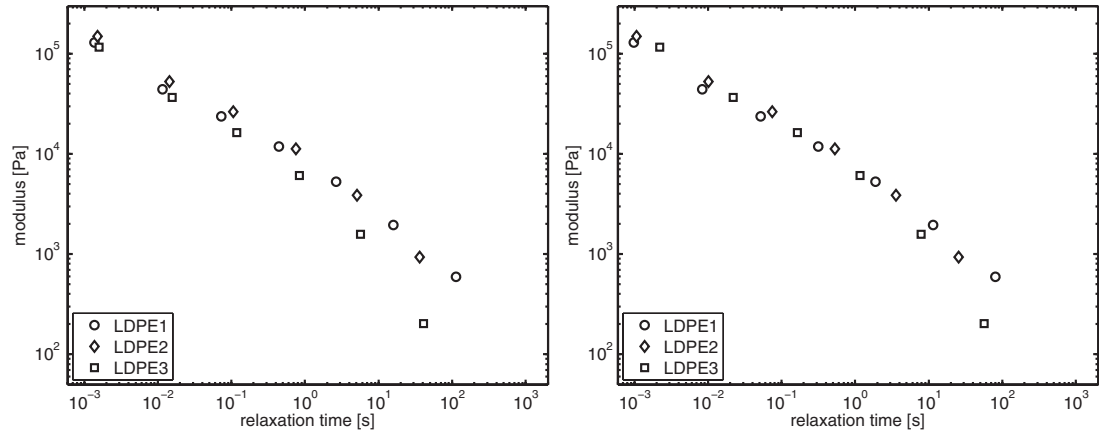

Figure 10. Maxwell spectrum: Moduli versus relaxation times for the three LDPE's at $T_{ref} = 190\ ^{\circ}C$ (a) and at process temperature (b), 200 °C for LDPE1 and LDPE2 and 180 °C for LDPE3, respectively.

(strain hardening), with a larger onset time for LDPE3. As stated earlier, the melt temperature during processing was chosen such that the rheological behavior is nearly identical for the three grades for similar processing conditions. Rheological identical is defined here in terms of the Maxwell-spectra, e.g., relaxation modulus and time, which were determined from the rheological spectra in Figure 10. By changing the melt temperature during processing, these were made nearly the same, see Figure 10b compared to Figure 10a. Notice that the linear viscoelastic curve for the time dependent extensional viscosity also becomes the same for the three grades, see Figure 11b. The non-linear behavior can, of course, not be controlled.

3.3. Effect of Processing Conditions

For clarity we have separated the discussion on the effects of processing conditions from the influence of molecular differences between the three grades. The latter will be presented in the next section by using the same results but organized in a different way.

3.3.1. Crystallinity

Changing the processing conditions affects the crystallization process in two different ways: first by influencing flow-induced crystallization (already discussed in Section 3.1) and second by changing the thermal history, in particular the cooling conditions. Once the polymer melt flows through the die-exit, it will experience a level of cooling proportional to the film thickness, the temperature difference between the film and the surrounding air and the (average) velocity of the film. For example, increasing the blow-up ratio results in a decrease of the film thickness and, therefore, a (slightly) higher cooling rate.

Figure 12 shows, for all combinations of blow-up and take-up ratios, the measured crystalline fraction as function

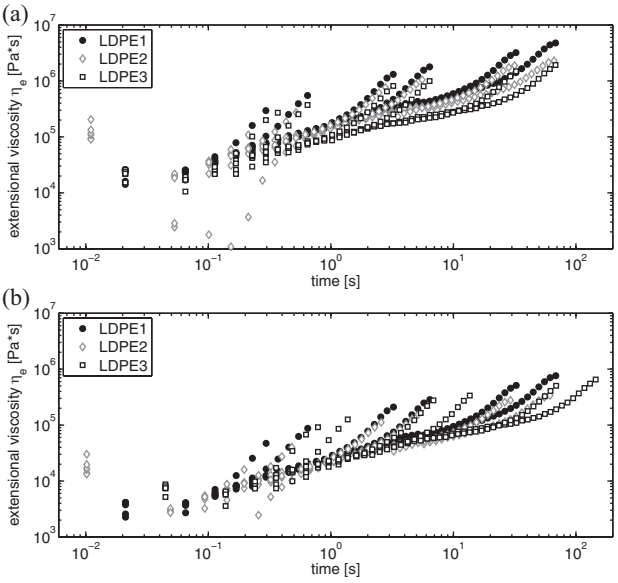

Figure 11. Extensional viscosity versus time for the three LDPE's at $T_{ref} = 150\ ^\circ C$ (a) and with data shifted to the process temperature (b), 200 °C for LDPE1 and LDPE2 and 180 °C for LDPE3, respectively. Strain rates are 0.05, 0.1, 0.5, 1, 5, and 10 s^{-1}.

of both, the distance and time elapsed since the melt left the die. Due to the height of the air-ring on top of the die, the minimum accessible distance measured from the die-exit is about 15 cm. The maximum distance from the die is constrained by the vertical displacement of the hydraulic lift table and, therefore, the point of full crystallinity development could not be captured, especially for high-TUR conditions. The position of the frost-line, determined from the velocity profile when possible, is also included in these figures.

For the low-BUR/low-TUR setting, which is considered as the "startup" condition in film blowing, crystallinity gradually develops with distance from the die and reaches a plateau value, just within the investigated window. With an increase of the TUR the crystallinity development takes place further away from the die. The opposite effect is achieved with increasing the BUR. The crystallinity versus time is rather instructive since it shows the evolution of the crystallization for the different conditions more clearly. From Figure 12b,d and f it is seen that, as expected, with higher molecular deformation caused by a higher TUR and/or BUR, the crystallization rate is enhanced. In fact, for all investigated grades, the fastest crystallization is observed for high-BUR/high-TUR conditions, followed by the low-BUR/high-TUR setting, the high-BUR/low-TUR and, finally, the low-BUR/low-TUR condition. This ranking of crystallization rates also evidences that, due to the higher values of axial strain rate in comparison with those in the tangential direction, TUR dominates over BUR in dictating the crystallization rate of the polymers.

With increased stress the frost-line also shifts toward a position closer to the die. It is evident that the frost-line does not mark a crystalline equilibrium state, but rather a degree of crystallization (approximately 15–20%) that transforms the material into the solid state. This indicates that even above the frost-line molecular re-arrangements can still take place. This result is in agreement with similar experiments performed by Ogale et. al. who observed a further sharp increase of the crystallinity closely beyond the frost-line.[27]

3.3.2. Molecular Orientation

An indicative measure for the orientation evolution of the crystalline structure is achieved by analyses of the FWHM of the (110) diffraction peak in the azimuthal direction. The results are presented in Figure 13. Notice that we present 1/FWHM instead of the FWHM since this shows the trends much more clearly. A sharp decrease in the FWHM of this peak is found at relatively small distances from the die-exit after which it reaches a plateau value. Such a decrease in FWHM is caused by an increasing fraction of oriented structures during solidification. It is clear that the observable development of structural features occurs in a very limited range, typically over a distance of about 5 cm, between 15 and 25 cm from the die exit.

Regarding the final FWHM level, a difference is found between high and at low TUR. The orientation at the maximum observable distance from the die is larger with higher take-up ratio, especially LDPE2 and LDPE3 show this effect clearly. A much smaller effect is found for the blow-up ratio. Just as observed for the crystalline content, TUR dominates over BUR in affecting the structure evolution. Regarding the position of the frost-line, measured at the point where the vertical velocity component becomes constant, it is observed that the frost-line is mostly located in the beginning of a final FWHM plateau region. This suggests that the frost-line could be a measure for the point where the overall molecular orientation level becomes constant.

For a more detailed picture of the orientation (i.e., at the level of the crystal lattice) we apply the Hermans' orientation factor. This analysis is here restricted to the results for LDPE1. When discussing similar results as a function of the molecular difference (next section), all grades will be taken into account. First, we show that for all experiments and materials, the CPO was found to be independent of the distance from the die, and averaged 0.43 ± 0.06 without significant deviations, see Figure 14. This result indicates that the experiments described in this study are resembling uniaxial conditions and molecular orientation can be described using Hermans' orientation factor.

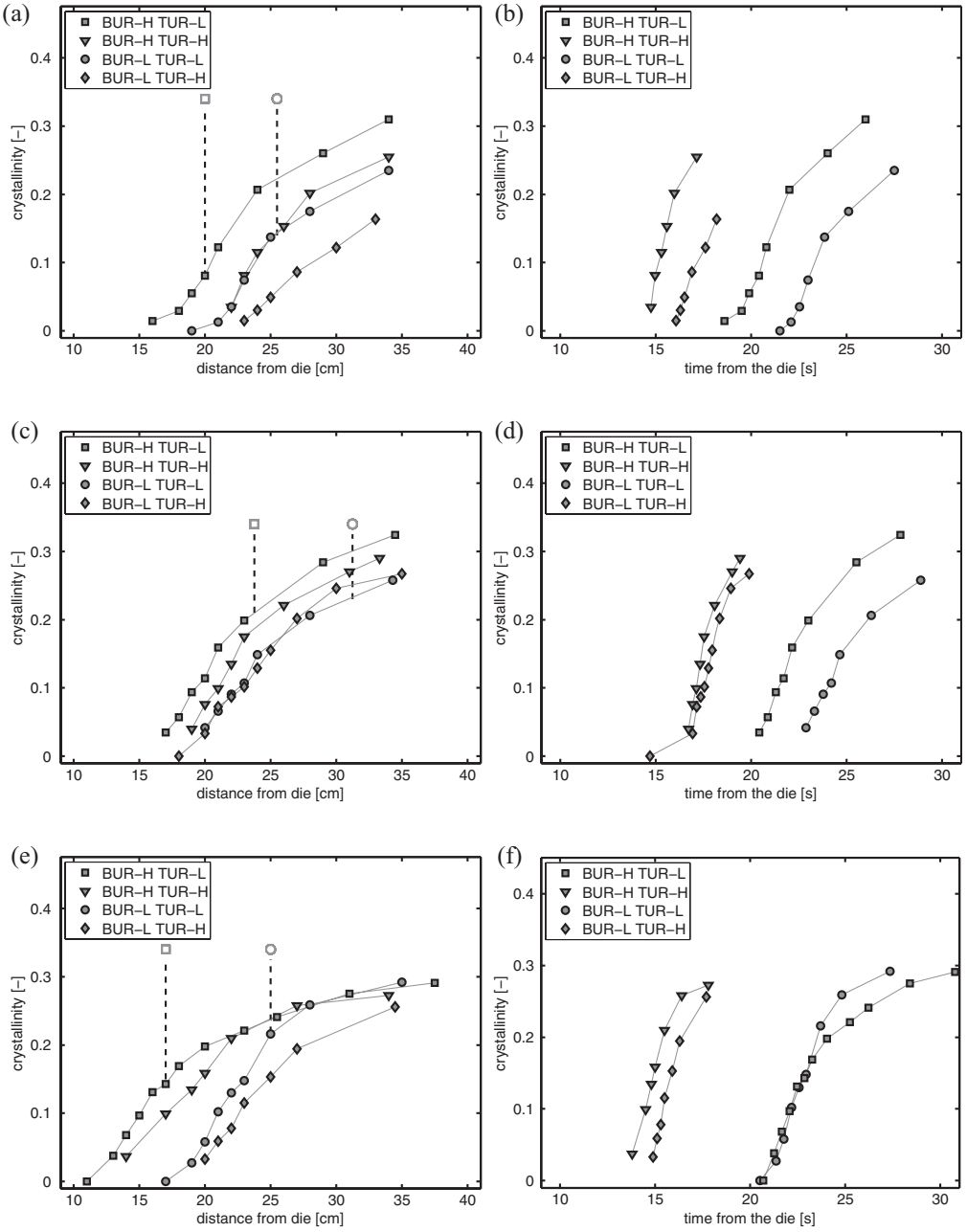

Figure 12. Crystallinity of LDPE1 (a,b), LDPE2 (c,d), and LDPE3 (e,f) versus distance from the die (a,c,e) and time from the die (b,d,f) for different processing conditions. Dashed vertical lines represent the position of the frost-line. Indices L and H represent high and low settings, respectively.

Figure 15 shows the orientation factors, f_a, f_b, and f_c, versus the distance from the die; results are displayed in a sub-figure for each combination of processing conditions. A moderate level of *a*- and *c*-axis orientation can be observed. The *c*-axis is already slightly oriented in the MD at relatively close distance to the die. From that distance onwards, the *a*-axis orientation increases at the expenses of the *c*-axis orientation. Meanwhile, the *b*-axis tends to become almost fully perpendicular to MD. In general, the molecular orientation in the flow direction is low (a value of 1 represents perfect alignment, f_c only reaches a value as much as 0.25). The level of f_c is indicative for the formation of oriented nuclei, row nuclei or/and shish and regular lamellae in the kebab (Type II). A positive final *c*-axis orientation, a negative final *b*-axis orientation and a moderate final orientation of the *a*-axis is found. The latter

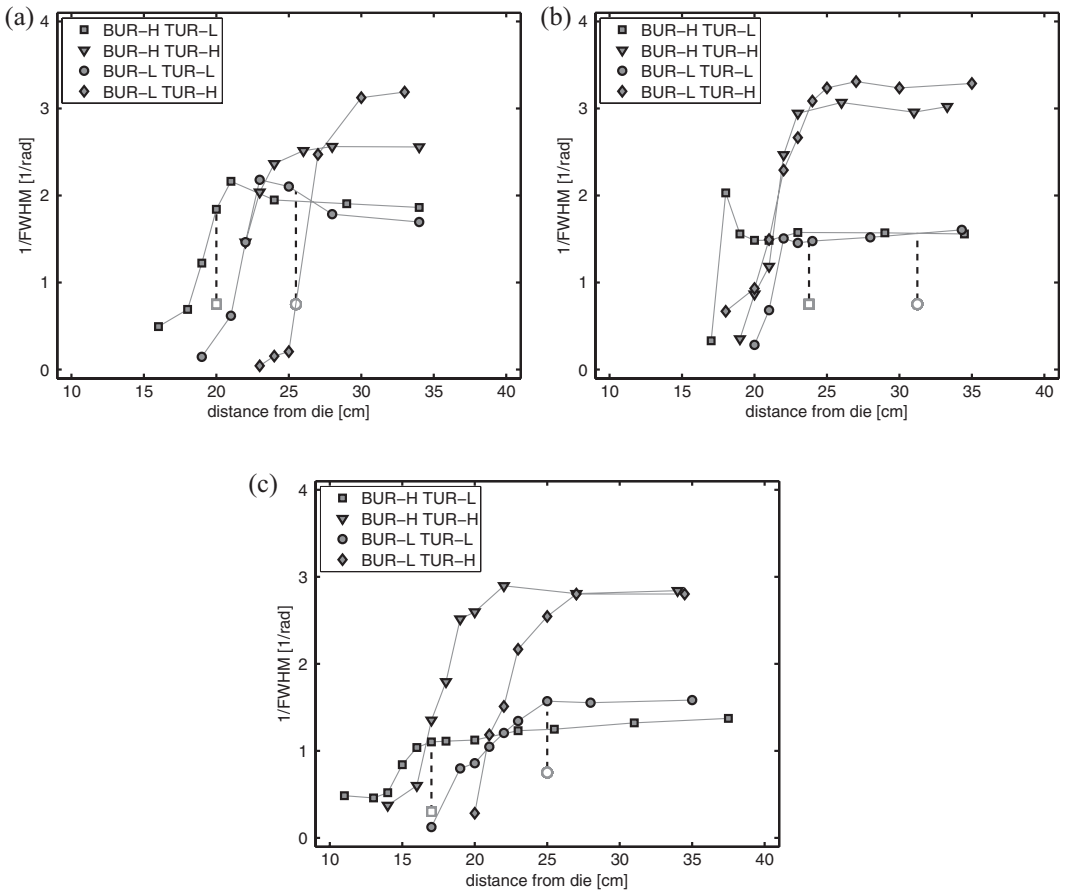

Figure 13. FWHM versus distance from the die for different processing conditions for (a) LDPE1, (b) LDPE2, and (c) LDPE3. Dashed vertical lines represent the position of the frost-line. Indices L and H represent high and low settings, respectively.

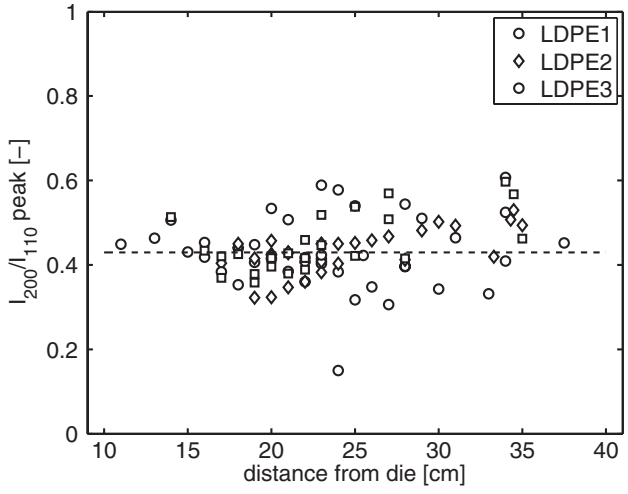

Figure 14. Peak ratio between the (200) and (110) reflection versus distance from the die for all materials and experiments investigated. The black dashed line represents the average value.

can be explained by the formation of twisted lamellae (Type I, see Figure 6) in the kebabs that contain, on average, a preferred *a*-axis orientation. Although it is reported that a high *a*-axis orientation not necessarily indicates Type I structures,[41] a larger number or size of the kebabs must increase f_a at the cost of f_c. Increasing the blow-up ratio at low-TUR shows no significant effect on the orientation of the crystallites. In the case of low-BUR/high-TUR conditions, a clear drop of the *c*-axis orientation is observed at larger distance from the die. This is accompanied with a pronounced *a*-axis orientation increase, marking the increase of the amount of twisted lamellae content at later stage. The difference between the evolution of f_c and f_a is best recognized for high-TUR conditions. No noticeable effect of applying different processing conditions is observed in the evolution of f_b, which always tends to approach a value between –0.25 and –0.3.

To confirm that the high *a*-axis orientation levels are a consequence of the presence of Type I morphologies, 2D

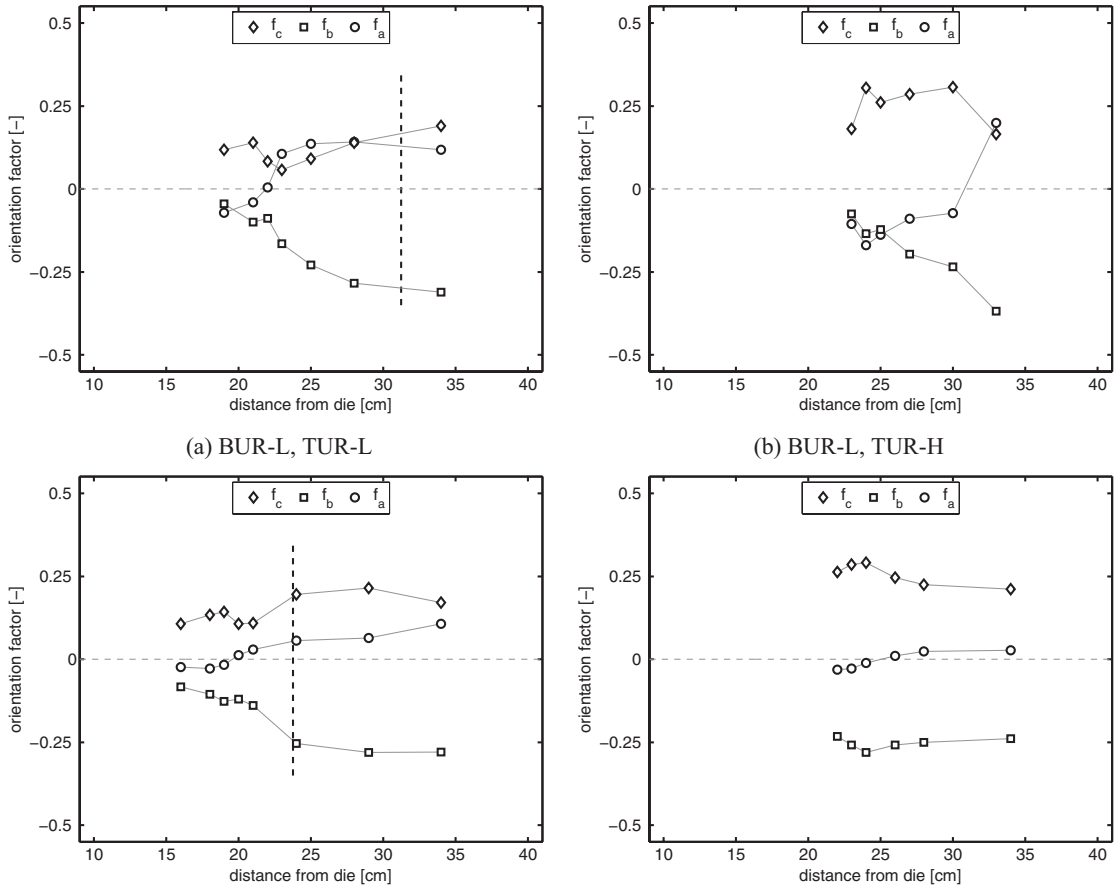

(a) BUR-L, TUR-L (b) BUR-L, TUR-H

(c) BUR-H, TUR-L (d) BUR-H, TUR-H

Figure 15. Hermans' orientation factor for LDPE1 for all molecular axes for each different processing condition with high (H) and low (L) blow-up ratio (BUR) and take-up ratio (TUR), respectively. Dashed vertical lines represent the position of the frost-line. Indices L and H represent high and low settings, respectively. On the plotted average values, a standard deviation of 0.04 should be taken into account.

WAXD patterns are compared for the minimum (low-BUR/low-TUR) and maximum (high-BUR/high-TUR) conditions, see Figure 16. The 2D diffraction images are taken at a maximum distance from the die.

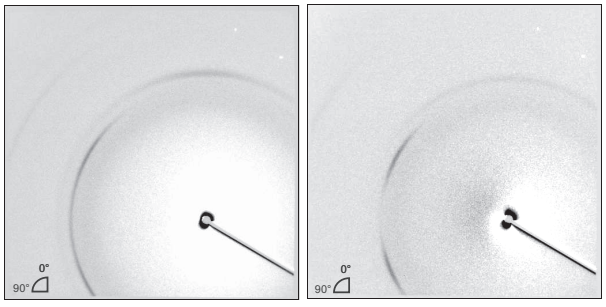

(a) TUR-L, BUR-L (b) TUR-H, BUR-H

Figure 16. 2D WAXD patterns for two extreme values of processing conditions for LDPE1, in the lower left corner the machine direction (0°) and transverse direction (90°) are indicated.

In both cases, there is indeed a clear sign of Type I structure formation, indicated by the (200) reflection located at 0° and the partitioned (110) reflection at 90°. Due to scattering from the front- and back-faces of the bubble, minor signs of the scattered front-face can be observed at high scattering angles.

The frost-line height, only available for the conditions presented in Figure 15a and c, shifts toward the die with an increase of the blow-up ratio. It is also observed that f_c seems to level off at the frost-line. This is supported by (but not a proof of) the results found by the FWHM analyses in Figure 13. One can notice that for the conditions in Figure 15b and d no frost-line could be detected within the range in which the deformation could be measured, and this is in agreement with f_c not leveling off.

As stated before, a large part of the crystalline fraction is formed beyond the frost-line position. A constant f_c indicates that the formation of row nuclei has ceased. Hence, the increase of crystallinity must be caused by the continuing growth of kebab structures, which increase the

overal crystallinity level and the average orientation of the a-axis in the flow direction. In additions, f_b evolves toward –0.5 by the continuous growth of the kebabs perpendicular to the direction of the shish. This observation will be discussed for the other polymers in the next section where the effect of molecular composition is compared.

3.4. Effect of Molecular Composition

3.4.1. Crystallinity

The development of crystallinity is compared for all grades per processing condition, see Figure 17. As stated before, this is the same data as presented in Figure 12a, c, and e, but rearranged in such a way that, if it is present, the effect of molecular features is highlighted. The sequential order in the crystallization rate of the three materials immediately becomes clear from the figure. For the conditions investigated, crystallization is found at closest distance from the die for LDPE3, closely followed by LDPE2 and, finally, LDPE1. The (mild) exception is seen for BUR-L/TUR-H where LDPE2 and -3 start to crystallize at the same position. However, is difficult to correlate this behavior to the material properties in Table 2. One has to remind that the three LDPE grades were extruded at different temperatures (see Table 2) in order to obtain similar rheological conditions during processing. LDPE3 was processed at 180 °C instead of 200 °C as for the other two grades and this can also cause the crystallization to take place slightly earlier in time and distance compared to the other materials. The results suggest that a relatively high $\overline{M}_w$ in combination with a relatively low $\overline{M}_w/\overline{M}_n$ (less content of UHM-chains, or high flow-ability) combined with a significant branching content, i.e., LDPE3, is most effective to achieve a high crystallization rate during the process. From these results we cannot draw any strong conclusion with respect to the final crystallinity level as a function of the molecular characteristics. One could speculate that, based on the higher density and the corresponding lower SCB, LDPE2 should reach a slightly higher final crystallinity level.

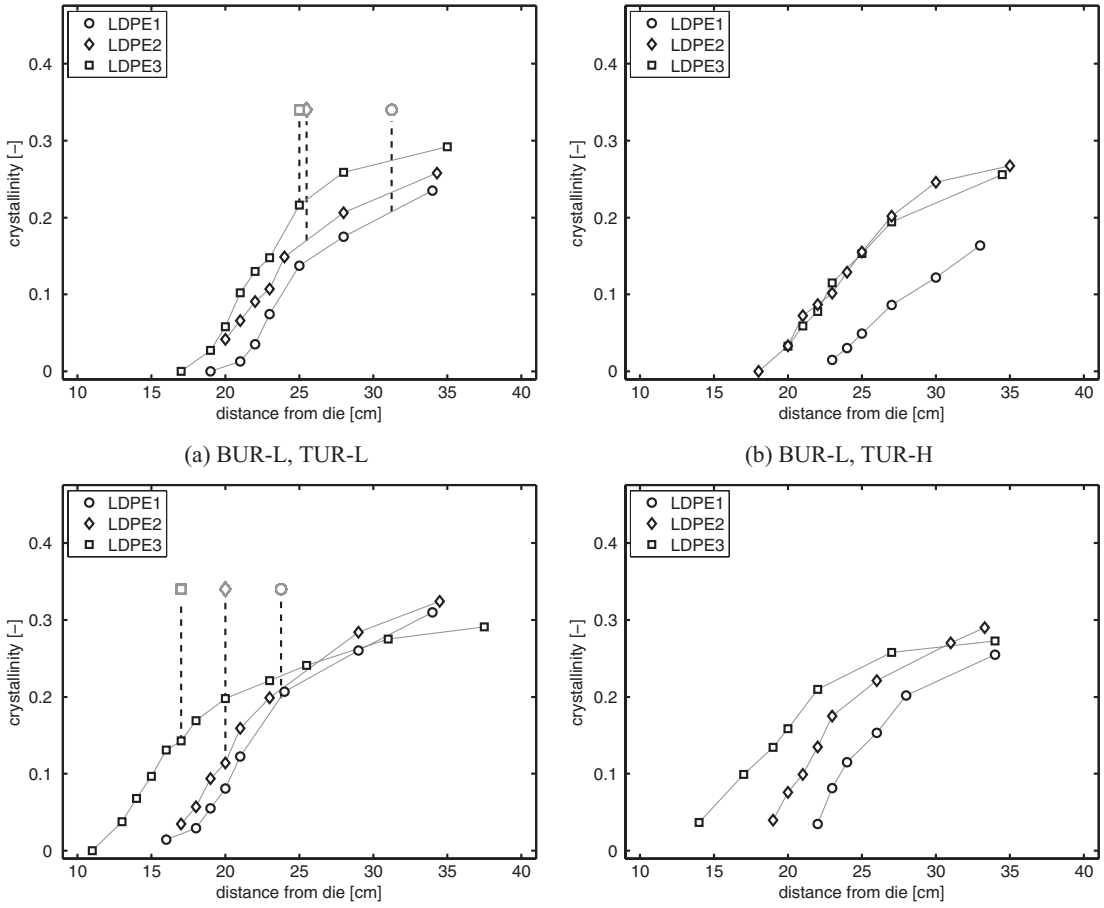

(a) BUR-L, TUR-L

(b) BUR-L, TUR-H

(c) BUR-H, TUR-L

(d) BUR-H, TUR-H

Figure 17. Crystallinity versus distance from the die for four different processing conditions. Dashed vertical lines represent the position of the frost-line.

Although such trend is observed for all cases except BUR-L/TUR-L, it is not really clear so we do not want to draw any strong conclusion on this. Independently of the LDPE grade the frost-line is observed at 20% and ≈15% crystallinity, for the low-BUR/low-TUR high-BUR/low-BUR and conditions, respectively.

3.4.2. Molecular Orientation

Once more, the full-width-at-half-maximum is used to provide an estimate of the development of orientation along the MD. This time, data of different materials is combined and plotted in a separate figure for each individual condition, see Figure 18.

Clearly, the development of orientation is strictly correlated to the occurrence of crystals, which can be deduced from the sharp decrease in FWHM. Similar to the results presented in Figure 13, LDPE3 shows the most rapid transition from the melt toward the oriented crystalline state. This is best observed in Figure 18d at close distance from the die. For the other two LDPE grades, the onset of crystallization is less clear, although LDPE2 appears to orient slightly faster.

From the data at large distance from the die it follows that the orientation levels scale with molecular weight. The polymer with the higher content of high molecular weight fraction, LDPE1, is able to strongly orient due to stretching, despite the slowest crystallization kinetics. LDPE3, having a slightly lower molecular weight content compared to LDPE2, develops the lowest level of orientation. Apparently, the rate of crystallization and the final level of orientation vary, as a function of molecular weight, in opposite directions. Considering the high-TUR processing conditions, the difference in orientation between the polymers is less pronounced, at least as can be distinguished using the FWHM method.

Since the FWHM method gives only a relative measure of the crystal orientation, the Hermans' orientation factor is

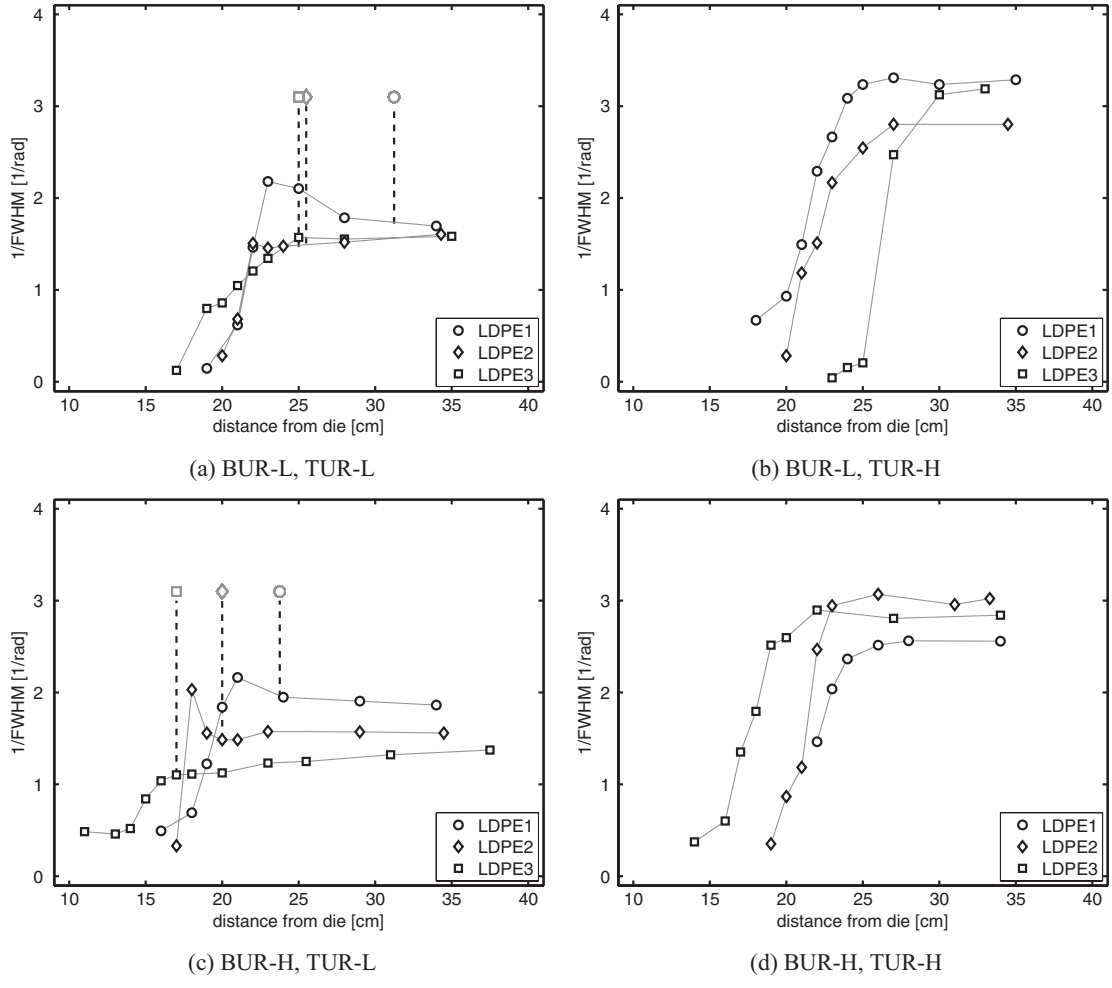

(a) BUR-L, TUR-L (b) BUR-L, TUR-H

(c) BUR-H, TUR-L (d) BUR-H, TUR-H

Figure 18. FWHM versus distance from the die for four different processing conditions. Dashed vertical lines represent the position of the frost-line.

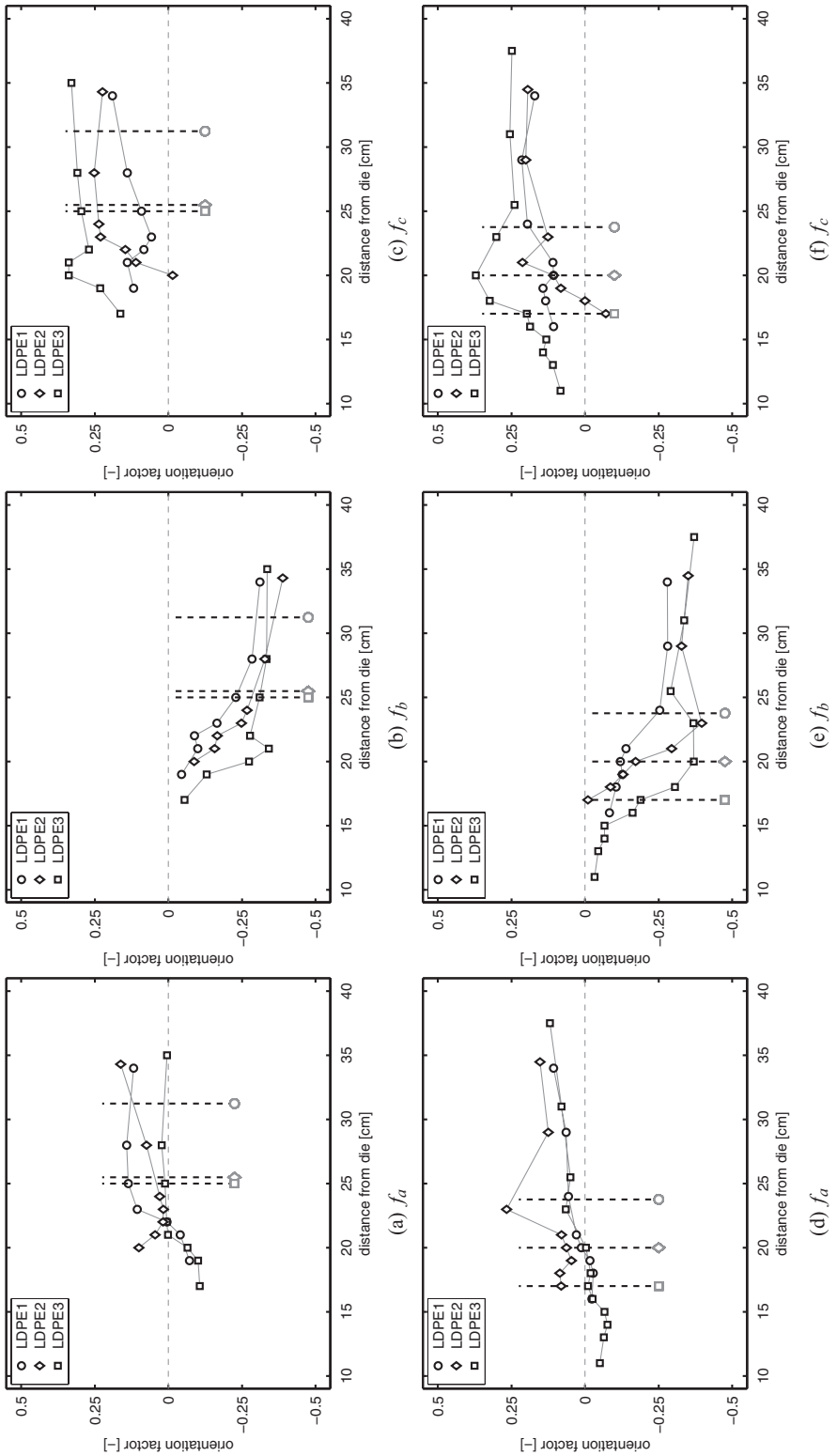

Figure 19. Hermans' orientation versus distance from the die for the three LDPE's, for BUR-L/TUR-L (top row) and BUR-H/TUR-L (bottom row). Dashed lines indicate the position of the frost-line. On the plotted average values, a standard deviation of 0.04 should be taken into account.

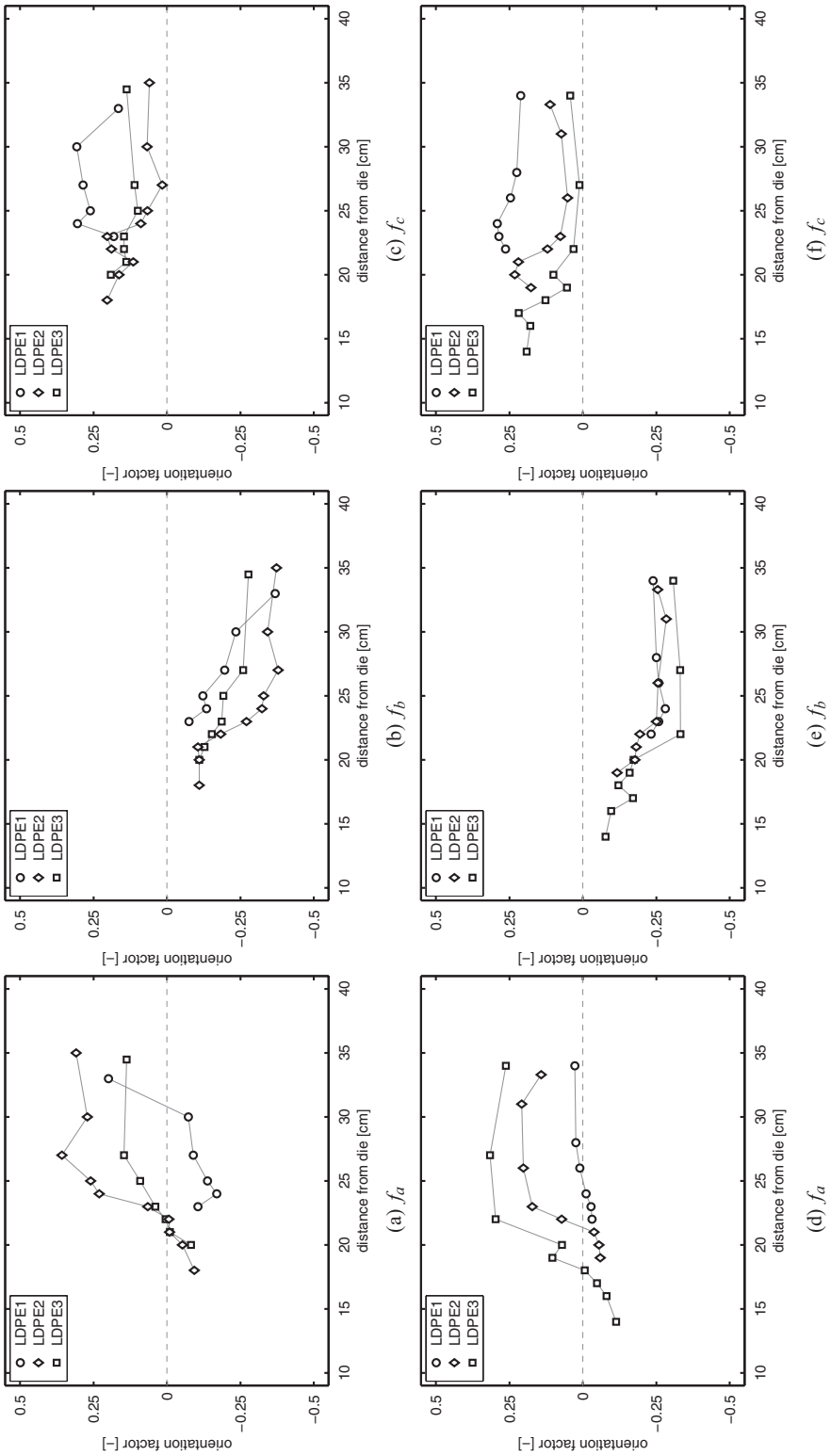

Figure 20. Hermans' orientation versus distance from the die for the three LDPE's, for BUR-L/TUR-H (top row) and BUR-H/TUR-H (bottom row). Dashed lines indicate the position of the frost-line. On the plotted average values, a standard deviation of 0.04 should be taken into account.

again used to further elaborate on the differences in the structure formation. This should allow us to draw more detailed conclusions on the influence of molecular composition on the orientation of each of the crystallographic axes and the relation of these with the frost-line height.

Data for each crystallographic axis are compared between materials for the different processing conditions, see Figure 19 and 20. For a low-TUR the results show some scatter, but a clear trend in the development of the orientation of the different axes is visible (see Figure 19). Both the *a*- and *c*-axis increase in the MD direction while the b-axis orientation is perpendicular to the bubble axis and tends toward –0.3. The orientation factors f_a and f_c are considered as most informative, since f_c indirectly acts as a measure for the mechanical properties in the machine direction,[43] and the balance between f_c and f_a gives an indication for the amount of lamellar twisting within the material. LDPE1 and LDPE2 show similar amounts of a-axis orientation where LDPE3 has a significantly lower value. Regarding the c-axis orientation, LDPE3 prevails, followed by LDPE2 and LDPE1, respectively. LDPE3 is highly oriented in the flow direction, which is (although we cannot be conclusive) though to be due to the high flow ability and the increased branching content.

For high-TUR, see Figure 20, remarkably high f_a values are found at low-BUR for LDPE2 and at high-BUR for LDPE3. Apparently, the *a*-axis orientation is very sensitive for a difference in branching contents upon an increase in BUR. For all high-TUR conditions, the highest *c*-axis orientation is noted for the high molar mass LDPE1. Meanwhile for LDPE3, the chain direction is only mildly oriented upon low-BUR, where an almost random orientation is observed at high-BUR. The opposite is found for LDPE2, where a low f_c is found at low-BUR, even smaller compared to the value at high-BUR.

It is quite evident that molecular features, such as average molar mass and content of branched repeating units, are reflected in how crystallization kinetics and crystal orientation are influenced by the deformation. However, at this stage, no unambiguous relation can be found between the orientation of the crystallographic axes, processing conditions and the molecular architecture of the polymer. It is clear that blown film extrusion is a complex process where non-isothermal crystallization is influenced by the thermo-mechanical history of the melt inside the die and the bi-axial stretching outside the die. The final result of this entire process is partly determined by the molecular architecture which influences the rheological behavior as well as the kinetics of crystallization. It is strongly believed by the authors that only a combination of extended material characterization (rheological, thermal, and flow enhanced crystallization kinetics)[44,45] and a full numerical model,[39,46–48] i.e., a model in which all of these aspects are included, will lead to a full understanding of these kind of experiments. On the other hand, such numerical simulations can only make sense when they are compared with the results of experiments at realistic processing conditions, such as presented here.

4. Conclusion

The experimental work reported in this paper demonstrates that combining blown film extrusion with synchrotron X-ray radiation enables one to acquire a full set of data describing the evolution of crystallinity and crystal orientation along the bubble, in the machine direction. For the designed set of processing conditions, it is demonstrated that, in terms of the influence on crystallization and orientation, the take-up ratio (TUR) dominates over the blow-up ratio (BUR). Moreover, a combination of a moderate $\overline{M}_w$ in combination with relatively low content of UHM-chains implies relatively high rates of crystallization, whilst a high molecular weight, as expected, leads to the highest overall orientation level. Also, it was observed that a high branching content and higher UHM fractions do not speed up crystallization. Due to the complexity of the film blowing process, a transient non-isothermal flow enhanced crystallization process with changing non-linear viscoelastic properties, no clear relation between material properties, and orientation of the crystallographic axes could be found. For the LDPE's studied and independent of both the material and processing conditions, the frost-line is observed at about ≈20% crystallinity. At this position also the final average orientation of the crystallographic *c*-axis is reached. Experimental results like these can help to understand and control polymer structuring in industrial practice and, moreover, can be used to validate results from numerical models for film blowing and help to improve and/or extend these models.

Acknowledgements: The authors would like to thank all people involved during the actual experiments at the ESRF. We would like to thank Dr. Dieter Lilge, Dr. Gerd Mannebach and Uwe Faller from LyondellBasell R&D, for providing the samples, performing the molecular characterization, the setup of the film-blowing line in Grenoble and the valuable input. Bob Fifield is acknowledged for his help with operating the film blowing setup. The Netherlands Organisation For Scientific Research (NWO) is gratefully acknowledged for access to the DUBBLE beamline. The Dutch Polymer Institute is acknowledged for continuing support for both the beamlines as well as enabling the research described in this work.

Received: May 6, 2014; Revised: June 20, 2014; Published online: August 22, 2014; DOI: 10.1002/mame.201400161

Keywords: crystal growth; in situ WAXD; low-density polyethylene; orientation; thin film

[1] G. Eder, H. Janeschitz-Kriegl, "*Processing of Polymers. Materials Science and Technology: A Comprehensive Treatment,*" *18*, Wiley VCH, Weinheim **1997**, Chapter 5, p. 269.
[2] H. Janeschitz-Kriegl, "*Crystallization Modalities in Polymer Melt Processing: Fundamental Aspects of Structure Formation,*" Springer, New York **2009**.
[3] Z. Bartczak, A. Galeski, A. S. Argon, R. E. Cohen, *Polymer*, **1996**, *37*, 2113.
[4] R. H. Somani, B. S. Hsiao, A. Nogales, S. Srinivas, A. H. Tsou, I. Sics, F. J. Balta-Calleja, T. A. Ezquerra, *Macromolecules* **2000**, *33*, 9385.
[5] J. M. Schultz, "*Polymer Crystallization. The Development of Crystalline Order in Thermoplastic Polymers,*" Oxford University Press, Oxford **2001**.
[6] R. H. Somani, L. Yang, L. Zhu, B. S. Hsiao, *Polymer* **2000**, *46*, 8587.
[7] J. Lu, H. Sue, T. P. Rieker, *J. Mater. Sci.* **2000**, *35*, 5169.
[8] B. A. G. Schrauwen, L. C. Av. Breemen, A. B. Spoelstra, L. E. Govaert, G. W. M. Peters, H. E. H. Meijer, *Macromolecules* **2004**, *37*, 8618.
[9] Z. Horvath, A. Manyhard, P. Doshev, M. Gahleitner, G. Voros, J. Varga, B. Pukanszky, *Appl. Mater. Interfaces 6*, 7456.
[10] A. Keller, M. J. Machin, *J. Macromol. Sci. (Phys.)* **1967**, *B1*, 41.
[11] X. M. Zhang, S. Elkoun, A. A. Ajji, M. A. Huneault, *Polymer* **2004**, *45*, 217.
[12] C. Silvestre, S. Cimmino, M. Raimo, D. Duraccio, B. del Amo Fernandez, P. Lafuente, V. Leal Sanz, *Macromol. Mater. Eng.* **2006**, *291*, 1477.
[13] A. Keller, H. W. H. Kolnaar, "*Flow-Induced Orientation and Structure Formation,*" Wiley VCH, Weinheim **1997**, Chapter 4, p. 189–266.
[14] R. J. Pazur, R. E. Prud'homme, *Macromolecules* **1996**, *29*, 119.
[15] A. Ajji, X. Zhang, S. Elkoun, *Polymer* **2005**, *46*, 3838.
[16] A. Ghaneh-Fard, *J. Plast. Film Sheeting* **1999**, *15*, 1941999.
[17] M. van Gurp, B. J. Kip, J. P. C. van Heel, S. de Boer, *J. Plast. Film Sheeting* **1994**, *10*, 156.
[18] C. J. S. Petrie, *Am. Inst. Chem. Eng.* **1975**, *21*, 275.
[19] X.-L. Luo, R. I. Tanner, *Polym. Eng. Sci.* **1985**, *25*, 620.
[20] I. A. Muslet, M. R. Kamal, *J. Rheol* **2004**, *48*, 525.
[21] S. Sarafrazi, F. Sharif, *Intern. Polym. Process.* **2008**, *23*, 30.
[22] J. S. Lee, H. W. Jung, J. C. Hyun, *J. Rheol.* **2011**, *55*, 257.
[23] A. K. Doufas, *Rheol. Acta* **2014**, *53*, 269.
[24] M. D. Bullwinkel, G. A. Campbell, D. H. Rasmussen, J. Krexa, C. J. Brancewitz, *Intern. Polym. Process.* **2001**, *16*, 39.
[25] G. Gururajan, A. A. Ogale, *J. Raman Spectrosc.* **2009**, *40*, 212.
[26] A. Ghaneh-Fard, P. J. Carreau, P. G. Lafleur, *Int. Polym. Process.* **1996**, *12*, 136.
[27] G. Gururajan, H. Shan, G. Lickfield, A. A. Ogale, *Polym. Eng. Sci.* **2008**.
[28] G. Gururajan, A. A. Ogale, *Polym. Eng. Sci.* **2012**, *52*, 1532.
[29] W. Bras, *J. Macromol. Sci., Part B: Phys.* **1998**, *37*, 557.
[30] M. Sentmanat, B. N. Wang, G. H. McKinley, *J. Rheol.* **2005**, *49*, 585.
[31] Verband Deutscher Maschinen und Anlagenbau, "*Kenndaten für Die Verarbeitung Thermoplastischer Kunststoffe, Teil 1, Thermodynamik,*" Hansen, Munich **1979**.
[32] W. Bras, I. P. Dolbnya, D. Detollenare, R. van Tol, M. Malfois, G. N. Greaves, A. J. Ryan, E. Heeley, *J. Appl. Crystallogr.* **2003**, *36*, 791.
[33] G. Portale, D. Cavallo, G. C. Alfonso, D. Hermida-Merino, M. van Drongelen, L. Balzano, G. W. M. Peters, J. G. P. Goossens, W. Bras, *J. Appl. Crystallogr.* **2013**, *46*, 1681.
[34] J. J. Hermans, P. H. Hermans, D. Vermaas, A. Weidinger, *Rec. Trav. Chim.* **1946**, *64*, 427.
[35] R. S. Stein, F. H. Norris, *J. Polym. Sci.*, **1958**, *21*, 381.
[36] P. H. Lindenmeyer, S. Lustig, *J. Appl. Polym. Sci.* **1965**, *9*, 227.
[37] S. Rastogi, Y. Yao, S. Ronca, J. Bos, J. van der Eem, *Macromolecules* **2011**, *44*, 5558.
[38] Z. W. Wilchinsky, *J. Appl. Phys.* **1960**, *31*, 1969.
[39] H. Zuidema, G. W. M. Peters, H. E. H. Meijer, *Macromol. Theory Simul.* **2001**, *10*, 447.
[40] P. P. Tas, *Film Blowing: From Polymer to Product*, PhD Thesis, Eindhoven University of Technology, **1994**.
[41] W. F. Maddams, J. E. Preedy, *J. Appl. Polym. Sci.* **1978**, *22*, 2751.
[42] A. Alizadeh, L. Richardson, J. Xu, S. McCartney, H. Marand, Y. W. Cheung, S. Chum, *Macromolecules* **1999**, *32*, 6221.
[43] J. Lu, H. Sue, *Macromolecules* **2001**, *34*, 2015.
[44] M. van Drongelen, T. B. van Erp, G. W. M. Peters, *Polymer* **2012**, *53*, 4758.
[45] T. B. van Erp, L. Balzano, A. B. Spoelstra, L. E. Govaert, G. W. M. Peters, *Polymer* **2013**, *53*, 5896.
[46] X. Guo, A. I. Isayev, L. Guo, *Polym. Eng. Sci.* **1999**, *39*, 2096.
[47] A. K. Doufas, I. S. Dairanieh, A. J. McHugh, *J. Rheol.* **1999**, *43*, 85.
[48] F. J. M. F. Custódio, R. J. A. Steenbakkers, P. D. Anderson, G. W. M. Peters, H. E. H. Meijer, *Macromol. Theory Simul.* **2009**, *18*, 469.